ANNUAL REVIEWS

Annual Review of Nuclear and Particle Science

Extended Scalar Sectors

Jan Steggemann[1,2]

[1]CERN, CH-1211 Geneva 23, Switzerland; email: jan.steggemann@cern.ch

[2]Current affiliation: Laboratoire de Physique des Hautes Énergies, École Polytechnique Fédérale de Lausanne, CH-1015 Lausanne, Switzerland

Annu. Rev. Nucl. Part. Sci. 2020. 70:197–223

First published as a Review in Advance on July 15, 2020

The *Annual Review of Nuclear and Particle Science* is online at nucl.annualreviews.org

https://doi.org/10.1146/annurev-nucl-032620-043846

Keywords

extended scalar sectors, Higgs boson, Higgs couplings, minimal supersymmetric Standard Model, MSSM, two Higgs doublet models, charged Higgs bosons, heavy scalars, LHC

Abstract

Extended scalar sectors appear in various extensions of the Standard Model of particle physics, such as supersymmetric models. They are also generic extensions of the Standard Model and can address a number of its shortcomings. Direct searches for additional Higgs bosons and measurements of the 125-GeV Higgs boson, both of which provide insights into the different possible sectors, are carried out at the LHC. This review gives an overview of searches for the additional Higgs bosons and their implications for different models. The discussed analyses comprise searches for neutral and charged Higgs bosons that decay in various final states. In addition, the review summarizes the constraints from precision measurements, including in particular the observed couplings of the 125-GeV Higgs boson. While several models naturally incorporate a Higgs boson with couplings that are similar to the ones in the Standard Model, the measurements of the 125-GeV Higgs boson provide constraints on all considered extensions.

Contents

1. INTRODUCTION

In 2012, the ATLAS and CMS Collaborations discovered a Higgs boson (1, 2) that is consistent with the predictions of the Standard Model of particle physics (SM). The new boson is the only fundamental scalar that has been observed to date, and its discovery confirms the Higgs mechanism for electroweak symmetry breaking (3–5). Its mass was measured to be 125.09 ± 0.24 GeV based on LHC Run 1 data (6) and was confirmed by recent updates from the ATLAS Collaboration (7) and the CMS Collaboration, which has provided the single most precise measurement to date: a mass of 125.38 ± 0.14 GeV (8).

SM: Standard Model of particle physics

h_{125}: 125-GeV Higgs boson

H_{SM}: Higgs boson in the Standard Model

While the measurements of the production and decay rates of the 125-GeV Higgs boson (h_{125}) are thus far consistent with the predictions for the Higgs boson in the Standard Model (H_{SM}), there is no requirement for the Higgs sector to be minimal. Extended Higgs sectors can address some of the shortcomings of the SM. For example, the SM provides no dark matter candidate and no explanation for the matter–antimatter asymmetry in the universe, so there must be physics beyond the SM. On a more theoretical level, the hierarchy problem—and whether it is a problem—has puzzled physicists for a long time and continues to do so (9, 10). Moreover, the SM does not explain its own flavor structure, nor does it yield coupling unification at high scales.

The Higgs field in the SM forms a complex doublet under weak isospin SU(2). Larger scalar sectors that include a boson consistent with the h_{125} observation typically include this complex

doublet and add additional structure. There can be additional real or complex singlets, doublets, triplets, and so forth, or a combination of them. The extended Higgs sector also can be embedded in a larger theoretical scenario, such as supersymmetry (SUSY) or little Higgs models, or it can be extended to include dark matter candidates.

MSSM: minimal supersymmetric Standard Model

2HDM: two Higgs doublet model

This review focuses on what has been learned about extended scalar sectors from recent LHC data. The theoretical approaches can be divided into two categories—bottom-up and top-down approaches—both of which have inspired the experimental analyses. In bottom-up approaches, pure extended scalar sectors are explored in a general fashion and can be considered as low-energy representations of an unknown larger theory at higher scales. In top-down approaches, the extended scalar sector is an intrinsic part of a concrete larger theoretical scenario. While this review gives a broad overview of the status of extended scalar sectors after the Higgs boson discovery and various dedicated searches at the LHC, it does not include models with nonminimal *CP* violation or with tree-level flavor-changing neutral currents (FCNCs). Other general reviews have addressed various aspects in more detail, such as bottom-up model building (11), the impact of extended scalar sectors on the couplings of the SM-like Higgs boson (12), and the SM Higgs sector as well as extended scalar sectors (13, 14). There also have been numerous reviews of more specific models, which are referred to in this review when those models are discussed.

Extended scalar sectors have two main phenomenological consequences. First, they lead to additional states, which can come in the form of additional neutral and charged scalars (commonly referred to as additional Higgs bosons). These states can be produced directly at high-energy colliders or leave imprints in precision electroweak measurements. Second, extended scalar sectors generally lead to modified h_{125} couplings compared with the SM.

The most well-studied full model is the minimal supersymmetric Standard Model (MSSM) (15). The MSSM addresses several shortcomings of the SM: It provides a dark matter candidate, allows for the unification of the gauge couplings, and mitigates the hierarchy problem. The MSSM requires two complex Higgs doublets (as opposed to the SM, which requires one). Its Higgs sector is hence a so-called two Higgs doublet model (2HDM) that gives rise to four additional neutral and charged scalars. A yet more complex additional scalar sector is realized in the next-to-minimal supersymmetric Standard Model (NMSSM), which addresses the so-called μ problem of the MSSM and further reduces the hierarchy problem (16). It adds a complex singlet to the 2HDM of the MSSM and leads to two additional neutral scalars that are phenomenologically different from the ones in the MSSM (17, 18). Both the MSSM and the NMSSM naturally include a Higgs boson with couplings that are consistent with the H_{SM} couplings in parts of their parameter space (e.g., if the mass parameter of the additional Higgs bosons is chosen to be above several hundred GeV). In contrast, bottom-up models usually need more fine-tuning to yield an h_{125} candidate consistent with the H_{SM} couplings (however, this may not be a problem, in particular under the assumption that there is an unspecified larger theory at high scale).

In terms of bottom-up models, 2HDMs have been studied in great detail (19, 20). Part of the motivation comes from a specific 2HDM being part of the MSSM; other motivations include the possibility of explaining the baryon asymmetry in the universe and axion models. Various other extensions have been subject to experimental investigations as well, including an additional singlet, which can be considered as the simplest possible extension of the SM Higgs sector and can give rise to candidates for dark matter; 2HDMs with additional (real or complex) singlets; and additional triplets.

2. OVERVIEW OF THEORY AND PHENOMENOLOGY

The SM Higgs potential is given by

$$V_{\mathrm{SM}} = m^2(\phi^\dagger\phi) + \lambda(\phi^\dagger\phi)^2, \qquad 1.$$

where ϕ is a complex doublet field and $m^2 < 0$ (3–5). The potential can be reparameterized to give the vacuum expectation value $v^2 = -m^2/\lambda$, with $v \approx 246$ GeV and the Higgs boson mass $m_h^2 = -2m^2$ (14). Besides giving rise to a new scalar particle, the Higgs mechanism introduces masses for the weak gauge bosons and makes it possible to introduce mass terms for the fermions with the help of the so-called Yukawa couplings. The couplings of the Higgs boson to other particles are set by their masses: They are linearly proportional to fermion masses and proportional to the square of the mass for bosons.

Electroweak precision measurements are in excellent agreement with the SM Higgs sector and can be used to put generic constraints on extended scalar sectors. Any given model needs to fulfill custodial symmetry—that is, the tree-level relation $\rho = m_W^2/(m_Z^2 \cos^2\theta_W) = 1$, where θ_W is the weak mixing angle (21). The model also needs to agree with the measured values of the so-called oblique parameters S, T, and U (14, 22).

2.1. Additional Singlets

The simplest extension of the SM is the addition of a real or complex singlet. Besides simplicity, another reason to explore additional singlets is that they can give rise to a dark matter candidate (23–26). The Higgs potential with a real singlet field S can be written as

$$V = m^2\phi^\dagger\phi + \lambda_1(\phi^\dagger\phi)^2 + \mu^2 S^2 + \lambda_2 S^4 + \lambda_3\phi^\dagger\phi S^2 + (\kappa_1 S + \kappa_2 S^3). \quad 2.$$

When applying a $\mathbb{Z}_2$ symmetry (invariance under $S \to -S$), linear or cubic terms in the singlet fields in parentheses vanish. The neutral components of ϕ and S mix, induced by λ_3, to form two physical states, h and H, with $m_h^2 \leq m_H^2$ by convention. Both h and H can take the role of h_{125}. The ratio of the vacuum expectation values defines $\tan\beta = v/\langle S\rangle$. The gauge and mass eigenstates can be related by introducing the mixing angle α, which implies that h couplings to SM particles are suppressed by a factor $\cos(\alpha)$, and the H couplings are suppressed by $\sin(\alpha)$. Accordingly, complete decoupling happens for $\sin(\alpha) = 0$ if $h \equiv h_{125}$ and for $\cos(\alpha) = 0$ if $H \equiv h_{125}$.

The theory can be described by five physical parameters: m_h, m_H, v, $\tan\beta$, and α. Assuming that either m_h or m_H takes a value of 125 GeV, and with the vacuum expectation value of the Higgs doublet ϕ given by its SM value of around 246 GeV, three free parameters remain: α, $\tan\beta$, and $m_{H/h}$. The h/H branching fractions generally correspond to those of H_{SM} because all couplings are suppressed universally. The decay $H \to hh$ is possible if kinematically allowed; if h is the 125-GeV Higgs boson, this condition is fulfilled for $m_H > 250$ GeV. If the decay is present, there is an additional suppression of H decays to SM particles depending on the partial width of $H \to hh$, which in turn depends on $\tan\beta$.

In the case of a complex singlet field, S in Equation 2 is replaced by a complex field (27). Such a model gives rise to two instead of one additional (pseudo-)scalars, one or both of which can be candidates for dark matter depending on the phases of the model. Considering separately the real and complex parts of the singlet, mixing can occur between all three Higgs fields.

2.2. Two Higgs Doublet Models and the Scalar Sector of the Minimal Supersymmetric Standard Model

Because of their presence in SUSY models—the MSSM in particular—2HDMs are the most studied extended scalar sector.

2.2.1. General two Higgs doublet models. In 2HDMs, there are two Higgs fields, ϕ_1 and ϕ_2, both of which are complex doublets. The most general 2HDM contains 14 free parameters.

However, 2HDMs lead to FCNCs, which experimentally are severely disfavored. Constraints from FCNCs can be evaded by requiring that each Higgs doublet couple only to right-handed fermions of one charge by means of a global $\mathbb{Z}_2$ symmetry (natural flavor conservation), still allowing for it to be softly broken by the m_{12} term below. The number of free parameters is reduced by four after applying the $\mathbb{Z}_2$ symmetry and by two more when requiring that there is no tree-level *CP* violation, given the strong limits on non-SM *CP* violation (14).

With these symmetries, the Higgs potential reads as follows (19, 20):

$$V = m_{11}^2\phi_1^\dagger\phi_1 + m_{22}^2\phi_2^\dagger\phi_2 - [m_{12}^2\phi_1^\dagger\phi_2 + \text{h.c.}] + \lambda_1(\phi_1^\dagger\phi_1)^2 + \lambda_2(\phi_2^\dagger\phi_2)^2 + \lambda_3(\phi_1^\dagger\phi_1)(\phi_2^\dagger\phi_2) + \lambda_4(\phi_1^\dagger\phi_2)(\phi_2^\dagger\phi_1) + [\lambda_5(\phi_1^\dagger\phi_2)^2 + \text{h.c.}]. \quad 3.$$

The potential gives rise to five physical states: two *CP*-even Higgs bosons h and H (scalars), a *CP*-odd Higgs boson A (pseudoscalar), and two charged Higgs bosons $H^\pm$. The ratio of the vacuum expectation values of the two Higgs doublets, whose sum corresponds to the value in the SM, defines $\tan\beta$:

$$v_1^2 + v_2^2 = v^2 \rightarrow \tan\beta = v_1/v_2. \quad 4.$$

The free parameters in the model can be traded for the four masses of the additional Higgs bosons m_h, m_H, m_A, and $m_{H^\pm}$; the vacuum expectation value v; $\tan\beta$; the *CP*-even mixing angle α; and the softly $\mathbb{Z}_2$-breaking parameter m_{12}. As in the singlet models, either h or H can take the role of h_{125}. The couplings $k_{VV}^{h_i}$ of the additional *CP*-even scalars h_i to vector bosons V follow the sum rule

$$\Sigma_i(k_{VV}^{h_i})^2 = 1. \quad 5.$$

This relation also holds for models with an arbitrary number of additional singlets and doublets. As with the overall suppression of couplings in the singlet model, this relation implies that couplings to vector bosons can only be reduced compared with the SM, not enhanced.

In the Yukawa sector, one defines by convention that ϕ_2 induces the masses of the right-handed up-type quarks (u_R). With this relation, there are four different possible configurations for how the Higgs fields connect to down-type quarks (d_R) and leptons (ℓ_R). These relations are shown in **Table 1** and define four different types of 2HDMs, which are called type I, type II, lepton-specific (also called type X), and flipped (also called type Y). In the type I model, ϕ_1 is inert and does not couple to fermions. This implies that ϕ_1 can be completely decoupled from the SM at high $\tan\beta$, and the model becomes free of collider constraints.

The couplings of the neutral Higgs bosons to fermions and gauge bosons can be expressed in terms of the H_{SM} couplings, as shown in **Table 2**. The couplings of the charged Higgs bosons to fermions follow those of the A boson. The notation $g^{\Phi}_{f(\phi_{1/2})}$ indicates the couplings of the (additional) Higgs boson Φ to fermions that are connected to $\phi_{1/2}$ in a given type of 2HDM, as can be inferred from **Table 1**.

Table 1 Connection of fermions to doublets in the four types of two Higgs doublet models with natural flavor conservation

Model	u_R	d_R	ℓ_R
Type I	ϕ_2	ϕ_2	ϕ_2
Type II	ϕ_2	ϕ_1	ϕ_1
Lepton-specific	ϕ_2	ϕ_2	ϕ_1
Flipped	ϕ_2	ϕ_1	ϕ_2

Table 2 Neutral Higgs boson couplings to fermions and gauge bosons at tree level normalized to the Standard Model Higgs boson couplings

Φ	$g^{\Phi}_{f(\phi_2)}$	$g^{\Phi}_{f(\phi_1)}$	g^{Φ}_{VV}
H_{SM}	1	1	1
h	$\cos\alpha/\sin\beta$	$-\sin\alpha/\cos\beta$	$\sin(\beta-\alpha)$
H	$\sin\alpha/\sin\beta$	$\cos\alpha/\cos\beta$	$\cos(\beta-\alpha)$
A	$\pm 1/\tan\beta$	$\tan\beta$	0

$f(\phi_1)$ and $f(\phi_2)$ indicate fermions connected to the fields ϕ_1 and ϕ_2, respectively.

The so-called alignment limit arises if one of the scalars becomes SM-like. The case $h \equiv h_{125}$ requires $\sin(\beta-\alpha) \to 1$, which has as a consequence $g^h_{VV} \to 1$ and $g^H_{VV} \to 0$. Similarly, the fermion couplings approach unity if $\sin(\beta-\alpha) \to 1$ unless either $\tan\beta$ or $1/\tan\beta$ is of comparable size to $1/\cos(\beta-\alpha)$. Taking the type II 2HDM as an example and assuming $\tan\beta \gg 1$, the hVV and $ht\bar{t}$ couplings are SM-like, whereas the $hb\bar{b}$ and $h\tau\tau$ couplings approach their SM values more slowly for $\sin(\beta-\alpha) \to 1$. The considerations for the case $H \equiv h_{125}$ are similar.

The alignment limit naturally arises for $h \equiv h_{125}$ if the masses of the additional Higgs bosons are much larger than that of h_{125}, $m_{A,H,H^\pm} \gg 125$ GeV (28). This is the so-called decoupling limit. However, alignment without decoupling can also be reached by a specific choice of parameters for either the heavy or the light scalar corresponding to the SM-like Higgs boson (29, 30).

2.2.2. Minimal supersymmetric Standard Model. The MSSM is the SUSY extension with minimal particle content and minimal gauge group (15, 31, 32). The MSSM also assumes R-parity conservation, which conserves lepton and baryon numbers in the superpotential and leads to a stable lightest superpartner. To cancel chiral anomalies, and because conjugate superfields cannot be used in a SUSY Lagrangian, the MSSM requires two complex doublet scalar fields of opposite hypercharge. These two doublets give mass separately to up-type and down-type fermions. The MSSM Higgs sector hence corresponds to a type II 2HDM, with the tree-level MSSM Higgs sector automatically conserving *CP* such that the neutral Higgs mass eigenstates are states of definitive *CP*.

In contrast to a general type II 2HDM, there are relations between the 2HDM parameters in SUSY models. The couplings in Equation 3 are replaced by expressions that are given in terms of the gauge couplings. As a consequence, the MSSM provides the nontrivial prediction that there is an upper bound on the mass of the SM-like Higgs boson, which is less than m_Z at tree level and pushed up to around 140 GeV by radiative corrections for a high SUSY scale (33–37). This prediction implies that the discovery of an SM-like Higgs boson with a mass greater than 140 GeV would have excluded the MSSM. As in the 2HDM, both h and H can take the role of the SM-like Higgs boson. The couplings to vector bosons and fermions are the same as in a generic type II 2HDM (see **Table 2**).

The MSSM provides strict relations between the masses of the Higgs bosons. At tree level, the $H^\pm$ mass can be expressed in terms of m_A and m_W, $M^2_{H^\pm} = M^2_A + M^2_W$. Similarly, for $m_A \gg m_Z, m_H$ approaches m_A, $m^2_H \simeq m^2_A + m^2_Z \sin^2 2\beta$. This implies that, for sufficiently large m_A—that is, when approaching the decoupling limit—the additional Higgs bosons are nearly degenerate in mass.

Because of the relations among its parameters, the MSSM has fewer free parameters compared with a generic 2HDM. At tree level, the only free parameters are $\tan\beta$ and m_A, which are sufficient to describe most of the general phenomenology. Important higher-order corrections arise from the mass of the SUSY partner of the top quark (the stop squark) and the stop-mixing parameters. The value of $\tan\beta$ is conventionally chosen in the range $1 < \tan\beta < 60$, which follows from

assuming universal boundary conditions at a grand unification scale (38). If this assumption is dropped, values of tanβ outside of this range are possible as long as the top and b quark Yukawa couplings remain perturbative (15).

One other important difference with respect to generic 2HDMs is that decays into SUSY particles can be possible. The most important decays are into charginos and neutralinos; decays into SUSY partners of leptons, third-generation quarks, and gluinos are also possible, even though those are ruled out for a wide range of masses by direct searches for SUSY particles at the LHC (39–41). Superpartners also can contribute to production and decay—for instance, from stop and sbottom quark contributions to the loop in gluon fusion production.

In the decoupling limit, which is approached already for moderate values of m_A, the h couplings naturally approach the H_{SM} couplings (42, 43). Unlike in general 2HDMs, alignment without decoupling does not occur at tree level. With a certain amount of fine-tuning, the MSSM parameters can be chosen such that they allow alignment without decoupling following an accidental cancellation of tree-level and loop-level effects for narrow regions in phase space.

Various benchmark scenarios have been developed that yield an SM-like Higgs boson compatible with 125 GeV in a large part of the parameter space (44). At low tanβ, a higher SUSY scale is necessary to achieve a mass as high as 125 GeV for the SM-like Higgs boson. This parameter space is addressed by specific benchmark scenarios (45). An approximate approach is taken by another benchmark scenario, the so-called hMSSM (46–49), in which m_h is fixed at 125 GeV, it is assumed that the superpartners of the SM particles are too heavy for the additional Higgs bosons to decay into them, and only specific radiative corrections are considered. Under these assumptions, the hMSSM is completely described by the two parameters m_A and tanβ.

In light of negative results of the searches for superpartners at the LHC, SUSY models with a higher scale, such as split SUSY, are of increasing relevance (50–52). In particular, split SUSY can have superpartners at scales that are inaccessible at the LHC but that still have Higgs sectors that are accessible at LHC energies (53, 54).

2.3. Other Extensions

More complex models, such as a 2HDM with an additional singlet or a model with an additional triplet, typically reproduce at least part of the phenomenology of singlets and 2HDMs but can add interesting new phenomenology and profit from specific motivations (13, 14). The extension of 2HDMs with a real singlet is called the N2HDM. Compared with a 2HDM, the N2HDM leads to the presence of an additional neutral scalar, which can be light compared with h_{125}. The N2HDM can be motivated by providing a dark matter candidate when applying a $\mathbb{Z}_2$ symmetry on the 2HDM (55–57). With a broken $\mathbb{Z}_2$ symmetry on the 2HDM, there is mixing between the singlet and the 2HDM (58, 59). The singlet admixture leads to an additional reduction of the h_{125} couplings, as discussed in Section 2.1 for the singlet case.

The extension of 2HDMs with a complex singlet is called 2HDM+S (60, 61); compared with the N2HDM, this model has an additional pseudoscalar a. The model can be parameterized by the six masses, four mixing angles, and three vacuum expectation values (v, tanβ, and v_S, with S denoting the complex singlet). An important phenomenological consequence of the N2HDM and 2HDM+S models is that Higgs-to-Higgs boson decays become more relevant because of the larger number of Higgs bosons and because the additional Higgs bosons may be as light as a few GeV.

The NMSSM is another well-studied full model that addresses some of the shortcomings of the MSSM (17, 18). It has only moderate fine-tuning compared with the MSSM and provides an explanation for the Higgsino mass parameter being near the electroweak or the SUSY-breaking

scale—that is, it addresses the μ problem of the MSSM (16, 62). It also allows the SM-like Higgs boson to have a mass of 125 GeV at low tanβ without having to resort to a high SUSY scale. The Higgs sector of the NMSSM is a type II 2HDM+S. Compared with a generic 2HDM+S, in the NMSSM, decays of the additional Higgs bosons into superpartners—in particular into invisible ones—are possible (63). Another interesting aspect is that the NMSSM generally leads to increased Higgs self-coupling, yielding potentially increased di–Higgs boson production rates (64).

Adding additional triplets generally violates custodial symmetry. Some mechanism is thus necessary to evade this constraint. Triplets can, for instance, be a consequence of left–right symmetric models and can generate neutrino masses. The Georgi–Machacek model solves the problem of violated custodial symmetry by aligning the vacuum expectation values of a real and a complex scalar Higgs triplet field, at the expense of additional fine-tuning (65, 66).

The main consequences of models with triplets are the presence of doubly charged Higgs bosons; the possibility of charged Higgs bosons decaying in the WZ final state; the presence of a fermiophobic additional scalar (67); and the possibility that the h_{125} coupling to vector bosons exceed their SM values, which is not the case in the other extended scalar sectors (68).

3. DIRECT SEARCHES FOR ADDITIONAL HIGGS BOSONS

The different models introduced in Section 2 give rise to neutral and charged Higgs bosons, which in turn decay into various final states based on their mass and couplings. Neutral additional Higgs bosons, either scalar (H, h) or pseudoscalar (A, a), can decay to heavy gauge bosons, photons, fermions, or a combination of Higgs bosons and heavy gauge bosons. **Table 3** provides an overview of the relevant decay modes in several models. Similarly, singly or doubly charged Higgs bosons decay in a number of ways, as summarized in **Table 4**. The large number of final states has motivated many searches at the LHC.

Most analyses can be carried out and reported in a model-independent way because there are typically only one or two relevant production mechanisms and the reconstructed width is often larger than the intrinsic width of the Higgs particle. The probed mass spectrum ranges from the GeV range to beyond 1 TeV for analyses in the $\tau\tau$ final state. Given the electroweak production process, the typically accessible mass is on the order of a hundred to a few hundred GeV—well

Table 3 Overview of the decay modes of additional neutral Higgs bosons that are either possible and relevant (■), possible but experimentally not relevant (•), or impossible (□) in a given extended scalar sector without explicit *CP* violation

	H	A/H				Higgs-to-Higgs			
Model	VV[a]	$\gamma\gamma$	$\tau\tau$	$b\bar{b}$	$t\bar{t}$	$H \to hh$[b]	$H \to AA$[c]	$A \to Zh$[d]	$H \to h_{125}h$[e]
Real singlet	■	•	•	•	•	■	□	□	□
2HDM	■	■	■	■	■	■	■	■	□
2HDM+S	■	■	■	■	■	■	■	■	■
Triplet	■	■	■	■	■	■	■	■	■

Abbreviations: 2HDM, two Higgs doublet model; 2HDM+S, two Higgs doublet model with a complex singlet.
[a] VV denotes WW or ZZ.
[b] $H \to hh$ comprises $H \to h_{125}h_{125}$ and $h_{125} \to hh$, depending on the mass hierarchy.
[c] Also includes $h_{125} \to AA/aa$ (the latter in 2HDM+S and triplet models).
[d] Also includes $A \to ZH$, $H \to ZA$, and the related decay $A/H \to WH^{\pm}$.
[e] Also includes $A \to h_{125}a$.

Table 4 Overview of the most relevant decay modes for charged Higgs bosons that are either possible (■) or not possible (□) in a given extended scalar sector without explicit *CP* violation

Model	$H^{\pm}$				$H^{\pm\pm}$	
	$\tau\nu$	tb	WZ	$(A/H)W$	$\ell\ell$	WW
Real singlet	□	□	□	□	□	□
2HDM	■	■	□	■	□	□
2HDM+S	■	■	□	■	□	□
Triplet	■	■	■	■	■	■

Abbreviations: 2HDM, two Higgs doublet model; 2HDM+S, two Higgs doublet model with a complex singlet.

below the LHC collision energy. The searches are hence statistically limited and will profit from increases in the integrated luminosity.

Despite the rich phenomenology, the searches share common patterns. In many cases, the decay products of the additional scalar particles can be fully reconstructed in the detector. Hence, a given analysis typically looks for a resonant enhancement over the background from SM processes—a search that is often referred to as a bump hunt. If the decay products decay further (i.e., if there are intermediate resonances in the decay), one can make use of their assumed masses by applying additional selection criteria or by using a kinematic fit to improve the resolution of the reconstructed mass of the additional heavy Higgs boson. If there are neutrinos or other particles escaping direct detection (e.g., in decays of τ leptons or W bosons), they can be detected in the transverse plane as missing p_{T} (69, 70). One may be able to infer the longitudinal component by exploiting the known mass of the intermediate particle (e.g., the W boson). If this is not possible—for instance, if there are several neutrinos—kinematic quantities in the transverse plane such as transverse mass often provide the best means by which to suppress the background.

The searches discussed below are based on LHC data taken in Run 2, which lasted from 2015 to 2018. The LHC provided proton–proton collisions at a center-of-mass energy of 13 TeV. Most results are from the ATLAS and CMS Collaborations and use at least the data recorded up to 2016, resulting in an integrated luminosity of at least ∼35 fb^{-1} and up to ∼140 fb^{-1} for analyses using the full Run 2 data set (71, 72). These results surpass the searches carried out with LHC Run 1 data because of both the larger center-of-mass energy and the larger amount of integrated luminosity.

3.1. Searches for Heavy Scalars and Pseudoscalars

Heavy neutral scalars and pseudoscalars can be produced via gluon fusion, in association with a b quark, or via vector boson fusion (VBF). The gluon fusion process, $gg \to A/H$, proceeds via a loop with the main contributions typically from top quarks except when the b quark coupling becomes large (e.g., at high $\tan\beta$ in the MSSM). In full models, contributions from other particles such as superpartners can become relevant. The b quark–associated production, $b\bar{b}A/H$, is most important for models that have enhanced couplings to fermions. Typically, at most one of the final-state b quarks remains in the detector acceptance. The VBF process is most relevant for models that have suppressed couplings to fermions.

3.1.1. Searches for scalars decaying to vector bosons or photons. Searches with vector boson pairs in the final state are important in all considered models, in particular in models with additional singlets and triplets, whereas searches in the diphoton final state are most relevant in models with a scalar or pseudoscalar mass around 100 GeV.

VBF: vector boson fusion

τ_h: hadronic τ decay

3.1.1.1. H → WW and H → ZZ. Searches for $H \to WW$ are in principle relevant whenever $H \to ZZ$ is relevant since the ratio of the Higgs couplings to vector bosons is universal in the considered models. For these searches, interference effects between signal and SM backgrounds are important and are taken into account. The searches in both final states also separately target gluon fusion and VBF production.

The most sensitive searches for $H \to WW$ for $m_H < 400$ GeV (73, 74) consider final states with an electron and a muon; beyond 400 GeV, final states with one charged lepton and two jets are more sensitive. In the lepton-plus-jets channel, it is possible to reconstruct the invariant mass of the WW system, which serves as the final discriminant. In the dilepton final states, a mass variable is reconstructed from the two leptons and the missing p_T vector.

Compared with $H \to WW$, the $H \to ZZ$ analyses profit from a superior mass resolution for a number of final states, but they suffer from a branching fraction that is smaller by at least a factor of two, and from smaller branching fractions of the Z boson decays to leptons. In general, the model-dependent limits are comparable to those of $H \to WW$ searches. Three final states—4ℓ, $2\ell 2\nu$, and $2\ell 2q$—are relevant and have been analyzed by the ATLAS and CMS Collaborations (75–77) (in this case, leptons include electrons and muons).

3.1.1.2. A/H → γγ. While the $A/H \to \gamma\gamma$ branching fraction is subdominant, the searches in this final state profit from an excellent mass resolution and manageable backgrounds, which make this final state particularly important for lower masses, for which searches in other final states are challenging. In addition, the relative branching fraction compared with the SM—where the W boson and top quark contributions to the loop cancel each other to a large extent—can be enhanced. Searches have been carried out for $m_{A/H}$ near 125 GeV in the context of the H_{SM} analysis (78) as well as for higher masses ($m_{A/H} > 200$ GeV) (79, 80) and lower masses ($65/70 < m_{A/H} < 110$ GeV) (81, 82). Challenges in the low-mass analysis[1] arise from event triggering due to the lower p_T of the photons and from the $Z \to ee$ background near m_Z.

3.1.2. Searches for scalars and pseudoscalars decaying to fermions. Searches in the $\tau\tau$ final state cover the most phase space in 2HDMs and the MSSM; other final states provide sensitivity where the branching fraction to $\tau\tau$ is small or in specific models.

3.1.2.1. A/H → ττ. Searches for $A/H \to \tau\tau$ by ATLAS and CMS consider the four most important $\tau\tau$ final states, which are, in decreasing order of sensitivity at high mass, $\tau_h\tau_h$, $\mu\tau_h$, $e\tau_h$, and $e\mu$, with τ_h denoting hadronic τ decay (86–88) and e and μ coming from a leptonic τ decay, $\tau \to \ell\nu\bar{\nu}$. Given the two τ leptons that have a large branching fraction to hadrons, the analysis requires excellent τ_h triggering, reconstruction, and identification, with multivariate methods applied both in ATLAS and CMS (89, 90). Both analyses use a combined transverse mass variable to search for the signal. **Figure 1** shows an illustrative distribution of the combined transverse mass variable for events in the $\tau_h\tau_h$ channel of the ATLAS search. The CMS analysis extends the search to masses as low as 90 GeV. Because the mass range of the CMS analysis includes the region around the h_{125} mass of 125 GeV, the predictions for all three neutral Higgs bosons (i.e., not only for H and A but also for h_{125}) are taken into account when interpreted in a given model.

3.1.2.2. A/H → tt̄. One of the main challenges in the searches for $A/H \to t\bar{t}$ involves the interference between SM $gg \to t\bar{t}$ and $gg \to A/H \to t\bar{t}$, which leads to pronounced peak-dip structures, with the relative sizes of the peak and dip parts depending on the coupling (92–96). The first

[1] A mild excess at 96 GeV has spurred some interest in the community (see, e.g., 83–85).

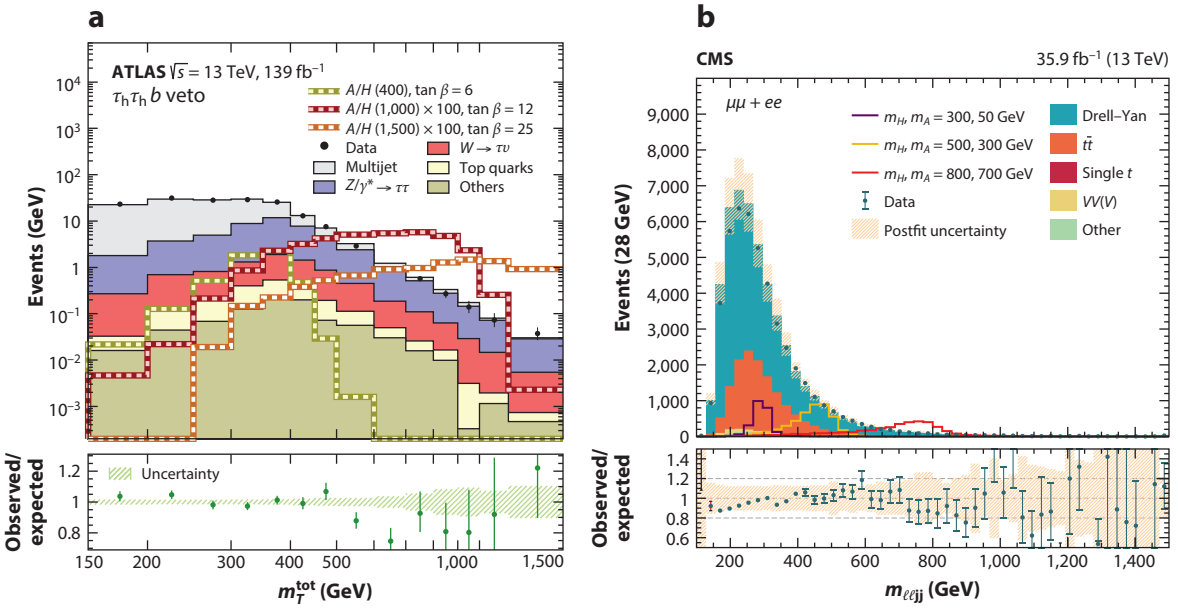

Figure 1

(*a*) Reconstructed distribution of a combined transverse mass variable, m_T^{tot}, in one of the considered event categories from a search for $A/H \to \tau\tau$. The background predictions are shown as stacked histograms, and exemplary signal distributions are shown as superimposed lines. The major backgrounds come from $Z/\gamma^* \to \tau\tau$ production at high m_T^{tot} values and from multijet production at low values. Compared with an $m_{\tau\tau}$ estimator, m_T^{tot} shifts backgrounds to lower values relative to the signal and increases the sensitivity of the search. (*b*) Distribution of the reconstructed mass of the two leptons and two *b* jet candidates in a search for $H \to ZA \to \ell\ell b\bar{b}$. For each considered signal hypothesis, elliptical regions in the $m_{\ell\ell b\bar{b}}$–$m_{b\bar{b}}$ plane are chosen to extract the signal. Panel *a* adapted from Reference 88 (CC BY 4.0). Panel *b* adapted from Reference 91 (CC BY 4.0).

experimental study at the LHC was a search by ATLAS for $m_{A/H} > 500$ GeV in final states with one reconstructed charged electron or muon and jets, looking at specific masses and widths (97). CMS followed up with a search in Run 2 for $m_{A/H} > 400$ GeV, including an interpretation in the hMSSM that fully takes into account the interference as well as the A/H mass splitting at low tanβ (98). The signal is extracted from the two-dimensional distribution of the reconstructed mass of the $t\bar{t}$ system and a final-state-dependent angular variable. A search has also been carried out for A/H production in association with $t\bar{t}$ in final states with two same-charge leptons or with more than two leptons; this search provides slightly weaker sensitivity (99).

***3.1.2.3.* A/H → bb̄.** Searches for $A/H \to b\bar{b}$ in *b* quark–associated production have been carried out by ATLAS and CMS (100, 101). The most sensitive final state is the one with three jets identified as *b* quark jets, given that the fourth *b* quark jet is rarely within the detector acceptance. The analyses rely on dedicated triggers that require identified *b* quark jets, and the signal is extracted from the reconstructed $b\bar{b}$ mass spectrum. While $\mathcal{B}(A/H \to bb)$ is five to nine times larger than $\mathcal{B}(A/H \to \tau\tau)$ for models with universal couplings to down-type fermions, the large background and small trigger acceptance make this search less sensitive than the ones for $A/H \to \tau\tau$.

3.1.2.4. Other fermionic final states. Both ATLAS and CMS also have looked for $A/H \to \mu\mu$ decays for $m_{A/H}$ starting from 130 GeV (102, 103). However, given the small branching fractions

due to the mass suppression for muons compared with τ leptons, these searches are significantly less sensitive than the ones for $A/H \to \tau\tau$ across the full tested parameter space.

Searches for A bosons at low mass ($25 < m_A < 60$–70 GeV) and produced in association with b quarks use $\tau\tau$ (104) and $\mu\mu$ final states (105). These searches are relevant in, for instance, 2HDMs with negatively signed Yukawa couplings to down-type fermions. There are also stringent limits in the mass range $0.2 < m_A < 9.2$ GeV, as observed by the BaBar Collaboration in a search for $A \to \mu\mu$ in Υ(1S) (106).

3.2. Searches for Higgs-to-Higgs Decays

Cascade decays of (additional) Higgs bosons including other Higgs bosons appear naturally in all extended scalar sectors if kinematically allowed. They often lead to a number of different final states that are relevant and are hence experimentally very rich.

3.2.1. Searches for $H \to h_{125}h_{125}$. With SM branching fractions of 58% to $b\bar{b}$, 21.5% to WW, 6.3% to $\tau\tau$, and 0.2% to $\gamma\gamma$, there emerge three $h_{125}h_{125}$ final states that, together, provide by a large margin the most sensitivity:

- The $b\bar{b}\gamma\gamma$ final state profits, on the one hand, from the large $\mathcal{B}(h_{125} \to b\bar{b})$ and, on the other hand, from the clean diphoton final state that leads to good background suppression, high mass resolution, and efficient triggering. This channel is most sensitive beyond the production threshold of $m_H = 250$ GeV up to around 400 GeV (107, 108).
- The $b\bar{b}\tau\tau$ final state has a larger branching fraction than that of $b\bar{b}\gamma\gamma$ but suffers from larger background and a more complex final state. Its sensitivity gets close to that of the $b\bar{b}\gamma\gamma$ final state at $m_H \gtrsim 350$ GeV and improves the combination at higher masses (109, 110).
- The $b\bar{b}b\bar{b}$ final state has the largest branching fraction but suffers from yet more background, in particular at low mass; it is also the most difficult to trigger because there is no clean lepton or photon in the final state. It provides the best sensitivity for $m_H > 400$ GeV (111, 112).

In general, the analysis strategy is to exploit the known h_{125} mass and to use m_{bb} (with b corresponding to the reconstructed h_{125}) as a final discriminant. By exploiting the known h_{125} mass, a significantly improved m_{bb} resolution is obtained in most of the considered analyses. Subleading channels have also been investigated, including $b\bar{b}WW$ (113, 114), $WWWW$ (115), and $WW\gamma\gamma$ (116). The most stringent limits are obtained in the ATLAS combination, which also provides interpretations in a model with an electroweak singlet and the MSSM (117).

3.2.2. Searches for $A \to Zh_{125}$. Searches for $A \to Zh_{125}$ are particularly relevant in the context of 2HDMs and extensions thereof, with most of the unique sensitivity between a kinematic threshold of $m_A \approx 220$ GeV and a $t\bar{t}$ threshold of around 350 GeV. In this mass range, $Z \to \ell\ell$ decays provide a clean handle to trigger the events and hence provide the best sensitivity. In terms of h_{125} decays, both $h_{125} \to b\bar{b}$ and $h_{125} \to \tau\tau$ provide similar sensitivity and are considered in the experimental analyses (118–120).

3.2.3. Searches for $A \to ZH$ and $H \to ZA$. Unlike the MSSM, extended scalar sectors may generally allow large mass splittings between A and H (e.g., in general 2HDMs), and the decays $A \to ZH$ and $H \to ZA$ can have large branching fractions and hence serve as important discovery channels. The most important final state is $\ell\ell b\bar{b}$. The A or H boson can be produced either by gluon fusion or by b quark–associated production in the relevant parameter space. Searches for

$A \to ZH$ and $H \to ZA$ have been reported by ATLAS and CMS (91, 121). The CMS analysis looks at mass ranges of 120 to 1,000 GeV for the heavier and 30 to 1,000 GeV for the lighter of the two additional Higgs bosons tested and is thus sensitive to the lighter additional Higgs boson being either lighter or heavier than h_{125}. For a given hypothetical A and H mass, some of the exclusive elliptical regions in the $m_{\ell\ell jj}$–m_{jj} plane centered on the expected reconstructed masses are used to define bins that are used for the signal extraction. The reconstructed $m_{\ell\ell jj}$ distribution is shown in **Figure 1**. Limits on the cross section times branching fraction are set in the m_H–m_A plane for mass splittings larger than the Z boson mass.

3.2.4. Searches for $h_{125} \to aa$. Decays of h_{125} into pseudoscalars a are relevant only if they are comparably light—that is, if m_a is less than half the h_{125} mass. This limits the experimentally relevant decay modes to $a \to \mu\mu$, $a \to \gamma\gamma$, $a \to \tau\tau$ (if $m_a \gtrsim 4$ GeV), and $a \to b\bar{b}$ (if $m_a \gtrsim 10$ GeV). The decays of the a boson to gluons or light quarks can have large branching fractions and typically dominate at lower a masses, but they have weaker sensitivity at the LHC for most of the considered models because of large backgrounds.

There are a few common experimental challenges. For lower m_a, the a boson is significantly boosted, which leads to its decay products being very close, making lepton and jet reconstruction and identification more difficult. Furthermore, the transverse momenta of the four final-state objects tend to be so small that it can be difficult to trigger the events, in particular for leptons from τ decays. Often, this also implies a low overall acceptance, which explains why final states with muons are often relevant despite their small branching fractions.

Searches for $h_{125} \to aa \to \mu\mu\mu\mu$ have unique sensitivity for $m_a < 4$ GeV (122, 123). A special challenge involves the backgrounds from quarkonia resonances. The CMS analysis explicitly models these backgrounds and considers the mass range $0.2 < m_{\mu\mu} < 9$ GeV, whereas the ATLAS analysis disregards dimuon masses in the vicinity of the quarkonia resonance masses but extends the considered $m_{\mu\mu}$ range to 20 GeV.

A search for $aa \to \mu\mu\tau\tau$ (124) for $3.7 < m_a < 50$ GeV selects two muons from one a boson decay, and either a reconstructed electron or muon from the decay of one of the τ leptons and one to three tracks from the other, to target hadronic τ decays with either one or three charged hadrons. Two different approaches exist in the search for both $aa \to \mu\mu\tau\tau$ and $aa \to \tau\tau\tau\tau$. The first search (125) targets the mass range $4 < m_a < 15$ GeV with a signature of two same-charge muons and two charged tracks, whereas the second search looks at the mass range $15 < m_a < 62.5$ GeV and considers the four fully reconstructed $\tau\tau$ final states $\tau_h\tau_h$, $\mu\tau_h$, $e\tau_h$, and $e\mu$ (126). A similar mass range of $15 < m_a < 60$ GeV is probed by a search for $aa \to bb\tau\tau$ that considers the $\tau\tau$ final states $e\mu$, $e\tau_h$, and $\mu\tau_h$ and requires at least one jet to be identified as a b quark jet (127). Searches for $aa \to \mu\mu bb$ look at a similar mass range of $18 < m_a < 62.5$ GeV and require both muons and b quark jets to be fully reconstructed (128, 129).

Other probed final states include $bbbb$ (130), $\gamma\gamma$+2 jets (131), and $\gamma\gamma\gamma\gamma$ (132). The final states with photons and/or gluons can become relevant in specific models in which a decays to fermions are strongly suppressed or forbidden, whereas the loop decays to photons or gluons can be possible via new states (133).

3.3. Searches for Charged Higgs Bosons

Singly charged Higgs bosons are mainly produced either via $t\bar{t}$ production and a subsequent $t \to H^{\pm}b$ decay, for $m_{H^{\pm}} + m_b < m_t$, or via $gg \to H^{\pm}tb$. A prediction at next-to-leading order for the transition region between the two production mechanisms around m_t, which previously had been disregarded by experiments, recently became available (134). For fermiophobic $H^{\pm}$ and $H^{\pm\pm}$ bosons, the most important production mechanisms are VBF and pair production. Beyond the

searches discussed below, a number of searches for other $H^{\pm}$ decays have targeted $t\bar{t}$ production with a $t \to H^{\pm}b$ decay, including searches for $H^{\pm} \to cs$ (135), $H^{\pm} \to cb$ (136), and $H^{\pm} \to WA$ (137).

3.3.1. Searches for $H^{\pm} \to \tau\nu$. Searches for $H^{\pm} \to \tau\nu$ are carried out in two lepton final states depending on the decay of the W boson: τ_{h} + jets or $\tau_{\mathrm{h}} + e/\mu$. The ATLAS search employs a multivariate discriminant as the final discriminant, using kinematic variables and an observable sensitive to τ polarization for lower masses, whereas the CMS search uses a transverse mass variable as the final discriminant in different categories based on jet multiplicities and kinematic observables (138, 139). In $t\bar{t}$ decays, an upper limit on $\mathcal{B}(t \to bH^{\pm}) \times \mathcal{B}(H^{\pm} \to \tau\nu)$ is obtained that ranges from 0.25% to 0.03% for $90 < m_{H^{\pm}} < 160$ GeV.

3.3.2. Searches for $H^{\pm} \to tb$. With two top quarks and two b quarks produced in the process, $gg \to H^{\pm}tb \to ttbb$, the final state is characterized by up to four reconstructed b quark jets and two W bosons. ATLAS and CMS performed very similar analyses in final states with two leptons, a single lepton, or jets only (140–142). In final states with leptons, the signal is searched for in the distribution of a multivariate discriminant in a number of categories defined by the numbers of jets and b quark jets.

3.3.3. Searches for $H^{\pm} \to WZ$. Searches for $H^{\pm} \to WZ$ assume VBF production and look at $m_H^{\pm} > 200$ GeV (143, 144). Looking at leptonic W and Z boson decays, the analyses require three leptons, a certain amount of missing p_{T}, and two jets with a large difference in pseudorapidity and fulfilling $m(\mathrm{jet}_1, \mathrm{jet}_2) > 500$ GeV to tag the VBF production mode. The ATLAS analysis fully reconstructs the neutrino using a W boson mass constraint and fits the reconstructed WZ mass, whereas CMS uses a transverse mass variable as the final discriminant.

3.3.4. Searches for doubly charged Higgs bosons. CMS has searched for doubly charged Higgs bosons ($H^{\pm\pm}$) decaying to two same-charge W bosons in VBF production (145). Final states are considered with two same-sign leptons (ee, $\mu\mu$, and $e\mu$), missing p_{T}, and two jets. Limits on the cross section are extracted from a fit to the two-dimensional distribution of dijet and dilepton mass for $m_{H^{\pm\pm}}$ ranging between 200 and 1,000 GeV.

Pair production of $H^{\pm\pm}$ with decays into WW has been studied by ATLAS in final states with two same-charge, three, or four leptons (146). Limits are set in the mass range of 200 to 700 GeV using optimized selection criteria in different event categories based on the missing p_{T} and a number of kinematic observables.

ATLAS also has searched for $H^{\pm\pm}$ pair production with direct decays to leptons in final states with two same-charge, three, or four reconstructed leptons (147). Preferred couplings to leptons can be achieved in, for instance, type II seesaw models in which the additional triplet gives rise to the neutrino masses, or in left–right symmetric models (148, 149). A fit is performed to the invariant mass distribution of the same-charge lepton pair in two-lepton and three-lepton final states and the average invariant mass of the two same-charge lepton pairs in four-lepton final states, and limits are extracted for $m(H^{\pm\pm}) > 200$ GeV.

4. CONSTRAINTS ON THE MINIMAL SUPERSYMMETRIC STANDARD MODEL

While the main focus of this review is on constraints from direct searches and measurements of the h_{125} properties, other important constraints arise and have to be satisfied. First and foremost, all tested models need to be theoretically feasible—for instance, they have to fulfill perturbative

unitarity and lead to a stable vacuum—which is implicitly assumed in the sections below. Second, the additional Higgs bosons can leave their imprints in precision measurements, such as the electroweak precision measurements alluded to in Section 2. In addition, constraints from a number of rare decays of b-flavored hadrons arise, including $B_s \to \mu\mu$, $B^+ \to \tau\nu$, and $B \to D^{(*)}\tau\nu$ (150). One of the most important constraints comes from the FCNC transition $b \to s\gamma$ and, in particular, from measuring the inclusive decay branching fraction $\mathcal{B}(B \to X_s\gamma)$ (151, 152). On the one hand, superpartners can contribute to the loop; on the other hand, SUSY-breaking terms can induce radiative corrections to the $H^\pm$ couplings to up- and down-type quarks (153). These constraints are considered in the benchmark models discussed below.

4.1. Constraints from Precision Measurements of the Standard Model–Like Higgs Boson

Measurements of the production and decay rates of h_{125} have been carried out by the ATLAS and CMS experiments (154, 155). For comparison with the MSSM, measurements of the couplings are considered that are expressed in terms of three parameters that involve the Higgs boson couplings to vector bosons, up-type quarks, and down-type quarks, as well as the total width of the Higgs boson. In the hMSSM, these parameters can be expressed analytically in terms of m_A and $\tan\beta$ (47–49). CMS obtains an expected lower limit on m_A that ranges from $m_A \gtrsim 390$ GeV at high $\tan\beta$ to $m_A \gtrsim 440$ GeV at low $\tan\beta$; the corresponding observed limits are tighter with $m_A \gtrsim 520$ GeV at high $\tan\beta$ and $m_A \gtrsim 600$ GeV at low $\tan\beta$. ATLAS obtains very similar expected and observed limits. At the current exclusion—for $m_A = 520$ GeV and at high $\tan\beta$—the branching fractions to WW, ZZ, and $\gamma\gamma$ in the hMSSM are around 11% below their SM values, whereas the branching fractions to $\tau\tau$ and $b\bar{b}$ are around 6% above the SM values, and the total width is 12% above. Tools have been developed that can use the coupling measurements to check their compatibility with arbitrary models (156–158).

4.2. Results from Direct Searches

Depending on m_A and $\tan\beta$, the decay branching fractions of neutral and charged scalars vary significantly—as do their production modes and cross sections—leading to a complex overall picture, as explained below.

4.2.1. Searches for neutral scalars. Neutral scalars in the MSSM are predominantly produced via gluon fusion, with the main contribution from a top quark loop at low and medium $\tan\beta$ and from a b quark loop at higher $\tan\beta$. The production cross section is similar to that seen in the SM at $\tan\beta = 1$, and then it falls with increasing $\tan\beta$; however, for $\tan\beta \gtrsim 10$, the b quark loop contributions and hence the overall cross sections are enhanced and become much larger than for SM-like production (for an exhaustive overview of the different calculations that are part of the predictions, see Reference 159). There are additional contributions from squark loops, which are of particular relevance in scenarios with a large mixing in the stop or sbottom sector. At high $\tan\beta$, b quark–associated production also plays an important role.

The search that covers the most phase space at medium and high $\tan\beta$ and for all values of m_A is the one for $A/H \to \tau\tau$, with the coupling scaling approximately with $\tan\beta$. The maximum value of $\mathcal{B}(A/H \to \tau\tau)$ is 15% at $m_A \gg 1$ TeV and $\tan\beta \approx 60$, while it vanishes for low $\tan\beta$ except for $m_A < 350$ GeV, where $\mathcal{B}(A \to \tau\tau)$ is still significant because $A \to t\bar{t}$ is kinematically inaccessible.

At low $\tan\beta$, several final states are relevant. Considering H decays, $\mathcal{B}(H \to WW)$ can reach more than 90% for $m_A < 150$ GeV and up to 50% for $\tan\beta \approx 1$ for $m_H > 250$ GeV, where

$H \to hh$ decays open up. The $H \to ZZ$ branching fraction can reach close to 30% for $m_A <$ 250 GeV and is slightly suppressed beyond. Finally, $\mathcal{B}(H \to hh)$ is up to 65% where it is kinematically accessible (i.e., for $m_H > 250$ GeV). As soon as $H \to t\bar{t}$ decays become accessible, their branching fraction is dominant—larger than 90% for $m_A = 400$ GeV and close to unity for high m_H. While $\mathcal{B}(H \to hh)$ can still reach several percent beyond the threshold, $\mathcal{B}(H \to WW/ZZ)$ is suppressed to the percent level near the threshold and drops steeply with increasing m_H.

For the heavy pseudoscalar A, decays to $t\bar{t}$ are even more dominant if kinematically open, given that decays to hh, WW, and ZZ are forbidden. Below the $t\bar{t}$ threshold, $\mathcal{B}(A \to Zh)$ can reach up to 83% for $\tan\beta \approx 1$ where kinematically accessible (i.e., for $m_A > 215$ GeV), with the branching fraction steeply falling with increasing $\tan\beta$. Otherwise, the decays $A \to bb$ and $A \to \tau\tau$ dominate, in proportions as given in Section 3.1.2.3.

4.2.2. Searches for charged scalars. The cross section for $gg \to H^{\pm}tb$ production falls with $\tan\beta$ up to $\tan\beta \approx 8$ and then rises again—similar to the production cross section for heavy neutral scalars (159–163). If kinematically accessible, the main branching fraction is to tb. $\mathcal{B}(H^{\pm} \to \tau\nu)$ is close to 1 when the decay to tb is not accessible, regardless of $\tan\beta$, and is still high for high $\tan\beta$ close to the tb threshold. For $m_A > 300$ GeV, $\mathcal{B}(H^{\pm} \to \tau\nu)$ becomes negligible at low $\tan\beta$ and makes up more than 10% for $\tan\beta > 10$ and up to 20% for $\tan\beta = 60$. For $H \equiv h_{125}$, the decay $H^{\pm} \to hW^{\pm}$ can become large (>90%) at low $\tan\beta$ if kinematically allowed, but this has not yet been searched for (44). Similar to neutral scalars, the $\tau\nu$ channel is more sensitive for most of the phase space because the tb channel suffers from larger background. However, for low $\tan\beta$, at which $\mathcal{B}(H^{\pm} \to \tau\nu)$ is negligible, the production cross section is high enough for the tb final state to become sensitive.

4.3. Summary of Constraints and Global Fits

The combined constraints on the scalar sector of the MSSM are summarized in terms of the parameters m_A and $\tan\beta$ in representative benchmark scenarios, distinguishing between the two cases where either h or H corresponds to h_{125}.

4.3.1. $h \equiv h_{125}$. The hMSSM exclusion in terms of m_A and $\tan\beta$ is shown in **Figure 2**. The plot includes constraints from searches for $A/H \to \tau\tau$, $H \to hh$, $H \to WW$, $H^{+} \to tb$, and $A/H \to t\bar{t}$. Searches for $A \to Zh$, $A/H \to b\bar{b}$, $A/H \to \mu\mu$, and $H^{\pm} \to \tau\nu$ provide weaker constraints than the results shown and have been omitted for visual clarity. The $A/H \to \tau\tau$ searches exclude a large region of parameter space at intermediate and high $\tan\beta$, with the exclusion reaching close to $m_A = 2{,}000$ GeV at $\tan\beta = 60$. For intermediate $\tan\beta$, where the production cross sections for additional Higgs bosons are smallest, the h_{125} coupling measurements provide the strongest constraints. At low $\tan\beta$, the constraints from h_{125} couplings are surpassed by exclusions from searches for $H^{\pm} \to tb$ and $A/H \to t\bar{t}$ near $\tan\beta = 1$, with the excluded region extending up to 700 GeV.

For several of the direct searches, constraints have also been obtained in other MSSM benchmark scenarios (44). While the general picture is similar to that of the hMSSM, the exclusions become a bit weaker in certain scenarios. For example, considering $m_A = 1$ TeV, the $A/H \to \tau\tau$ analyses exclude $\tan\beta \gtrsim 15$ in the hMSSM but only $\tan\beta \gtrsim 22$ in a scenario in which heavy Higgs boson decays into superpartners become relevant.

4.3.2. $H \equiv h_{125}$. The main exclusions from direct searches are from $H \to hh$ (low $\tan\beta$), from $H^{\pm} \to \tau\nu$ (for $M_{H^{\pm}} < 170$ GeV), and from $A/H \to \tau\tau$ (for $M_{H^{\pm}} > 170$ GeV). The search for

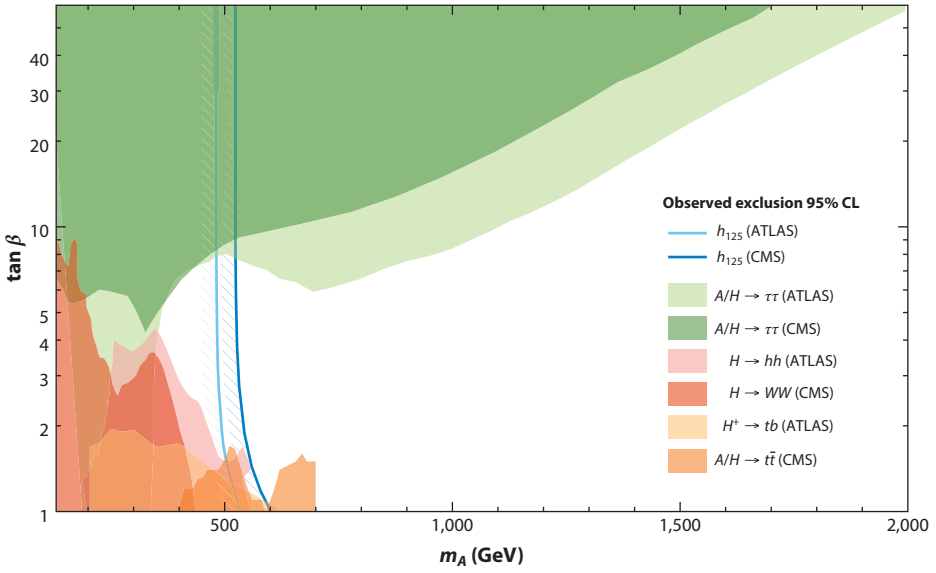

Figure 2

Observed exclusion at 95% CL in the hMSSM parameter plane m_A–tanβ from collider searches. Results from direct searches are shown as filled regions; searches were carried out by the ATLAS and CMS Collaborations and comprise searches for $A/H \to \tau\tau$ (87, 88), $H \to hh$ (117), $H \to WW$ (74), $H^+ \to tb$ (140), and $A/H \to t\bar{t}$ (98). The exclusions obtained from h_{125} coupling measurements are also shown (154, 155). The exclusion demonstrates the complementarity between the constraints from direct searches—which extend the excluded region beyond $m_A = 1$ TeV at high tanβ and up to $m_A = 700$ GeV at low tanβ—and constraints from the h_{125} coupling measurements that provide the most sensitivity at intermediate values of tanβ. The hMSSM is a benchmark scenario for the minimal supersymmetric Standard Model (MSSM) that assumes that the lower-mass scalar h corresponds to the observed 125-GeV Higgs boson (46–49). Other abbreviations: CL, confidence level; h_{125}, 125-GeV Higgs boson.

$H^\pm \to \tau\nu$ is particularly relevant in this case because $H^\pm$ bosons at low mass can be produced in $t\bar{t}$ decays. In addition, the h_{125} coupling constraints cover a similar region. Only a small bit of phase space remains open in a narrow region around $M_{H^\pm} \approx 160$–170 GeV and tan$\beta \approx 5.1$–5.7 (44, 153). In this region, the unsought decay $H^\pm \to hW^\pm$ has a large branching fraction.

4.3.3. Global fits. Fits of the MSSM parameter space have been performed that do not restrict themselves to the extended scalar sector, with a different number of free parameters (164, 165). In particular, constraints on direct searches for dark matter and from the relic density are taken into account. The results show a mild preference for heavy Higgs boson masses in the TeV range near the boundary of the considered phase space.

5. OTHER TWO HIGGS DOUBLET MODELS

5.1. Precision Observables

Like all other models, general 2HDMs need to fulfill theoretical constraints—in particular perturbativity of the couplings and vacuum stability, for which radiative corrections were recently studied (166). The oblique parameters also provide important constraints that apply equally to the different types of 2HDMs (167, 168). If $h \equiv h_{125}$, they require either m_A or m_H to be near

$m_{H^\pm}$. The allowed region becomes narrower when approaching the alignment limit, $\cos(\beta-\alpha)\to 0$, with a preference for both m_A and m_H to be near $m_{H^\pm}$.

Important constraints also arise from B decays (151, 152, 168–170). In type II and flipped models, the stringent limit $m_{H^\pm} > 590$ GeV is obtained from measurements of $B\to X_s\gamma$ decays. This constraint is more general than in the MSSM, in which superpartners can cancel the $H^\pm$ contributions. A complementary upper limit on $\tan\beta$ can be derived from $B_s\to\mu\mu$ decays in the type II model, with the upper limit on $\tan\beta$ ranging from 17 to 25 for an $m_{H^\pm}$ range of 590 to 1,000 GeV. In the type I, lepton-specific, and flipped models, the lower limit on $\tan\beta$ derived from $B_d\to\mu\mu$ ranges from 3 to 1 for an $m_{H^\pm}$ range of 125 to 1,000 GeV.

Constraints on the four types of 2HDMs from the h_{125} coupling measurements are obtained in a similar way as for the MSSM (see Section 4.1), using the results from ATLAS and CMS (154, 155). The obtained exclusions are shown in **Figure 3**. For all four types of 2HDMs, the main allowed region is near $\cos(\beta-\alpha)=0$, with the exclusion being least tight for $\tan\beta=1$ and tighter for $\tan\beta$ above and below 1, with the exception of the type I 2HDM, in which the constraints become weaker with increasing $\tan\beta$.

5.2. Direct Searches

As in the MSSM, direct searches for the additional Higgs bosons play an important role in 2HDMs. However, because of the larger parameter space, it is more difficult to draw general conclusions, and exclusions are obtained for specific choices of parameters. To point to peculiar features in certain areas of phase space, benchmark models have been proposed—for instance, for a few general cases (171) and for the specific case in which the masses of the heavy neutral Higgs bosons differ substantially (172).

In general, the conclusions obtained in the MSSM also hold for a type II 2HDM with a degenerate mass spectrum for the three heavy states (H, A, and $H^\pm$). One important difference is that the rates of $A\to Zh$, $H\to hh$, and $H\to WW/ZZ$ strongly depend on $\cos(\beta-\alpha)$ and approach zero in the alignment limit. This implies that searches for these final states can become more important than in the MSSM—in particular at low $\tan\beta$ and not too large m_A—or that alternative searches like $H^\pm$ searches in both tb and $\tau\nu$ final states or $A/H\to\tau\tau$ and $A/H\to t\bar{t}$ are most sensitive in this region.

The main feature of the flipped model compared with the type II model is that the lepton couplings are enhanced at low and not at high $\tan\beta$. The $A/H\to\tau\tau$ searches therefore do not exclude parameter space at high $\tan\beta$, and searches for $A/H\to b\bar{b}$ lead to the most stringent constraints (100, 101). In the lepton-specific model, the high $\tan\beta$ region is less constrained than in the type II model because the coupling to b quarks does not rise with $\tan\beta$, which leads to suppressed rates of both production via gluon fusion (where the b quark loop dominates at high $\tan\beta$ in the type II model) and b quark–associated production. Finally, the type I 2HDM is probed by $H\to WW/ZZ$, $H\to hh$, $A\to ZH$, and $A/H\to\tau\tau$ at low $\tan\beta$, with the relative importance depending on $\cos(\beta-\alpha)$ and $\tan\beta$. There is no sensitivity for larger values of $\tan\beta$ because the second Higgs doublet is inert.

For a nondegenerate mass spectrum of the three heavy states, processes like $H\to ZA$ and $A\to ZH$ become possible, with the decays also having high branching fractions for $\cos(\beta-\alpha)\to 0$. Therefore, direct searches for these processes can exclude a significant part of the phase space (91, 121). For models with a mass hierarchy, there are a few additional channels like $H\to WH^\pm$, $A\to WH^\pm$, $H^\pm\to WA$, and $H\to H^\pm H^\pm$ (171, 173). These processes remain largely uncovered experimentally, with the notable exception of a recent search for $H^\pm\to WA$ (137).

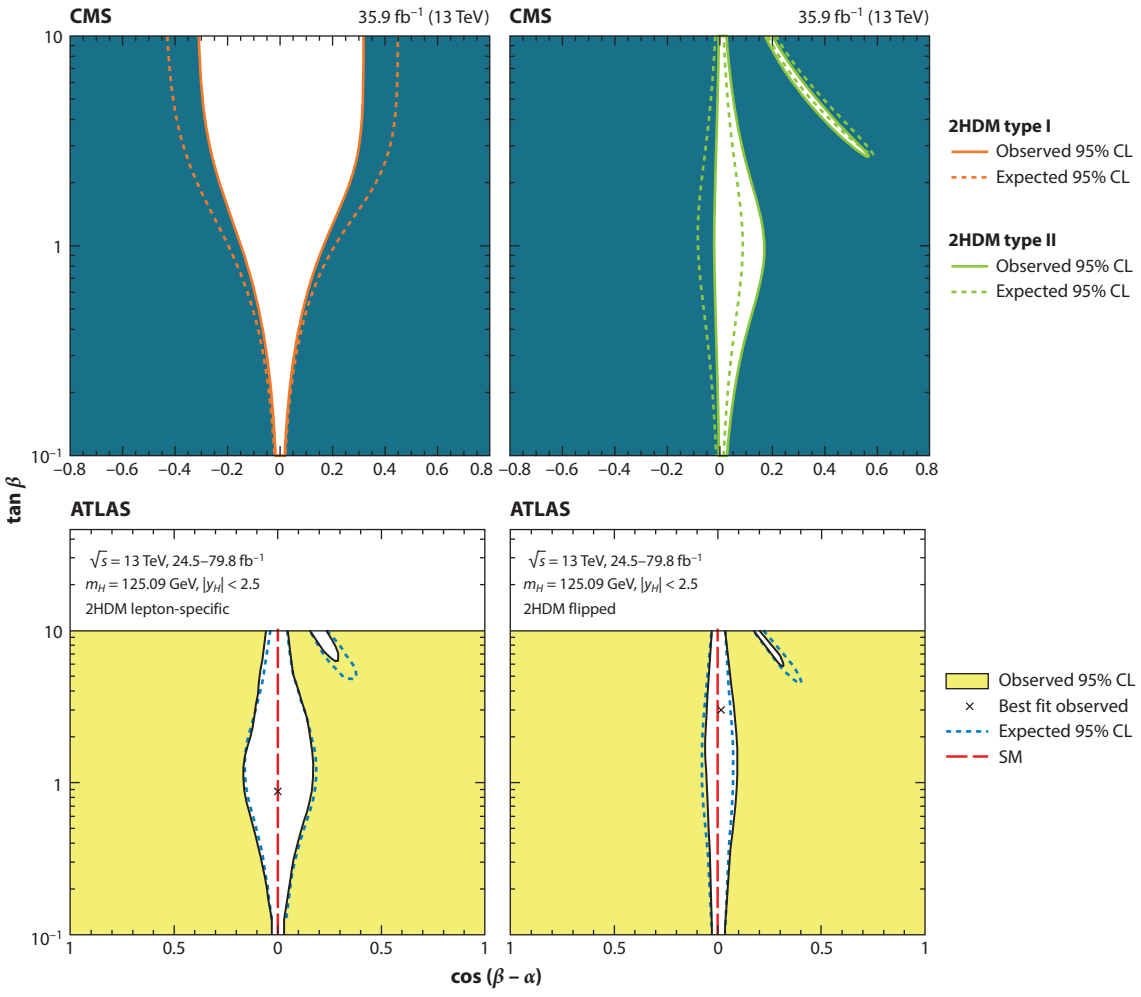

Figure 3

Exclusion in the tanβ–cos($\beta - \alpha$) plane in the four types of 2HDMs with natural flavor conservation from CMS (*upper panels*, *blue*) and ATLAS (*lower panels*, *yellow*) measurements of the h_{125} couplings. The contours for the type I and II models show the CMS results, whereas the contours for the lepton-specific and flipped models show the ATLAS results. Consistent results are obtained in the complementary cases. For all four types of 2HDMs, a large fraction of the parameter space is excluded, and the main allowed region is near the alignment limit of cos($\beta - \alpha$) $\rightarrow$ 0. The shape of the excluded region when tanβ varies is driven by the modified Yukawa couplings, which differ by type of 2HDM and increase roughly with either tanβ or 1/tanβ. In the type I 2HDM, the deviations of all Yukawa couplings become larger with decreasing tanβ such that the exclusion is weakest for large tanβ. In the type II, lepton-specific, and flipped 2HDMs, there is a second allowed region [for positive cos($\beta - \alpha$) and larger values of tanβ] that corresponds to solutions with negatively signed couplings to fermions, which are not yet excluded with the current measurements. Abbreviations: CL, confidence level; SM, Standard Model; 2HDM, two Higgs doublet model. Upper panels adapted from Reference 154 (CC BY 4.0). Lower panels adapted from Reference 155 (CC BY 4.0).

Combining results from precision measurements and from direct searches, recent global fits have been performed for the four types of 2HDMs with natural flavor conservation (168, 174) and for the inert 2HDM (175).

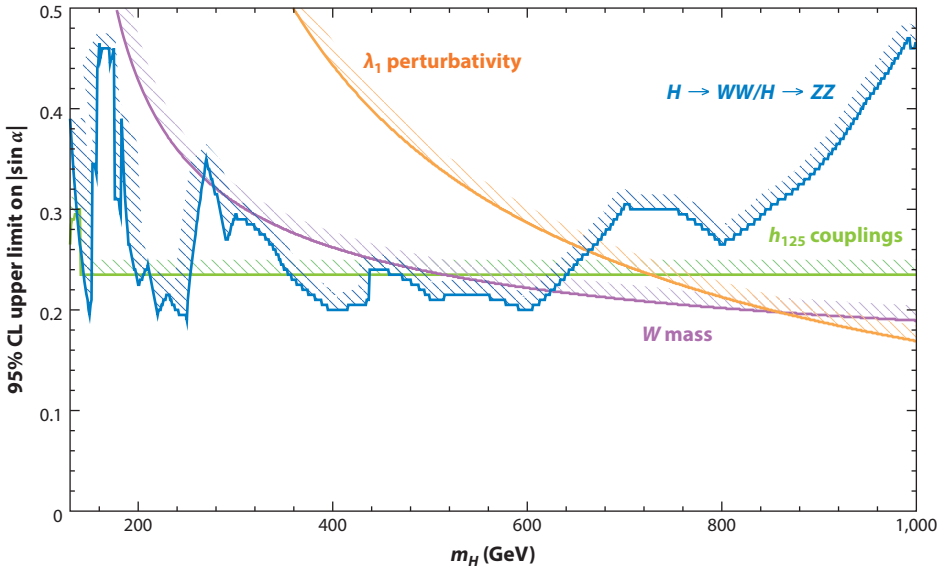

Figure 4

Exclusion in m_H–|sinα| plane in a model with a real additional Higgs singlet for tan$\beta = 1$ and with $h \equiv h_{125}$. Variation in tanβ will lead to variation in the $H \to hh$ partial width, which in turn varies the $H \to WW/ZZ$ branching fraction and thereby the exclusion curves by around ±30% for $m_H > 250$ GeV. Abbreviations: CL, confidence level; h_{125}, 125-GeV Higgs boson. Figure adapted from Reference 180 (CC BY-NC-ND 4.0).

6. OTHER EXTENSIONS

6.1. Additional Singlet

Constraints on the model with a real additional singlet arise from a number of sources. First, the additional singlet democratically reduces all $H_{\rm SM}$ couplings to SM particles proportional to cosα. Second, the heavy scalar H can be searched for, with the most sensitive searches being the ones for $H \to WW$, $H \to ZZ$, and $H \to hh$ decays. Third, constraints arise from the effect on electroweak precision observables, including the mass of the W boson (176). Finally, the model needs to fulfill theoretical constraints, in particular perturbative unitarity.

Figure 4 shows the resulting exclusion for tan$\beta = 1$, with inputs taken from References 177–180. Constraints from SM Higgs measurements are obtained from HiggsSignals-2.3.0 (156–158). The exclusion from searches for high-mass scalars decaying to vector bosons is taken from HiggsBounds-5.4.0 (181–184). In models without $\mathbb{Z}_2$ symmetry, larger branching fractions $H \to hh$ are possible (185).

6.2. Two Higgs Doublet Model with a Complex Singlet and Next-to-Minimal Supersymmetric Standard Model

As in the 2HDMs discussed above, electroweak precision observables require one of the additional Higgs masses in 2HDM+S models to be near $m_{H^\pm}$ (59). The constraints from measurements of the h_{125} couplings generally follow a pattern similar to that of generic 2HDMs, with an additional contribution from mixing with the additional singlet that leads to an overall reduction of the h_{125} coupling. The discussion here focuses on general 2HDM+S models, but all conclusions also apply to the NMSSM, for which several dedicated benchmarks have been proposed (159, 186, 187).

These models have a number of phenomenological consequences compared with 2HDMs. First, there is an additional scalar and an additional pseudoscalar, with the three scalars commonly denoted as h, h_{125}, and H and the two pseudoscalars as a and A. Notably, the additional neutral Higgs bosons h and a can be light—much lighter than h_{125} in particular. Second, heavy Higgs boson decays to lighter Higgs bosons are much more relevant, in particular because the cross sections for the production of the light states tend to be low since there is typically large mixing with the singlet. As in 2HDMs, h/H decays into WW and ZZ are suppressed in the case of alignment, as are $A \to Zh_{125}$ and $H \to h_{125}h_{125}$ decays (61). However, various other decays are unsuppressed and thus can have large branching fractions if kinematically allowed. These decays include those involving Z bosons ($H \to Za$, $A \to Zh$, and $h_{125} \to Za$), those involving three different Higgs bosons ($H \to h_{125}h$, $A \to h_{125}a$, and $A \to ha$), and those of heavier Higgs bosons into lighter ones ($H \to hh$, $H \to aa$, $h_{125} \to hh$, and $h_{125} \to aa$).

Several searches for additional Higgs bosons with masses below 125 GeV have been performed in the contexts of 2HDM+S and NMSSM models—most notably searches for a singlet-like Higgs boson decaying into two photons with $m_h < 125$ GeV (81, 82, 188) and a search for low-mass Higgs bosons in radiative decays of $\Upsilon(1S)$ (106) that set tight constraints on $\sin(\beta - \alpha)$ for $m_a < 9.5$ GeV (189). In addition, a number of searches have targeted the direct production of additional low-mass Higgs bosons (e.g., in $\mu\mu$ and $\tau\tau$ final states) (104, 105). However, these searches are experimentally challenging because of the large background and are typically only sensitive for very specific choices of parameters.

The Higgs-to-Higgs decays involving Z bosons discussed above apply in the same way when replacing H and A in the decay with their lighter counterparts h and a. In addition, the channel $H_{SM} \to ZA$ is addressed by recasting a search for dark Z bosons (122), which is particularly relevant in the lepton-specific and flipped 2HDM+S models (189). The decays involving three different Higgs bosons have not yet been searched for explicitly and would hence be among the most interesting next targets for searches at the LHC (187).

As discussed in Section 3.2.4, various searches have been performed targeting $h_{125} \to aa$ decays, with different final states being important for different a masses as different decay channels open. An overview of the exclusion obtained from these searches is shown in **Figure 5** for a type II 2HDM+S model with $\tan\beta = 2$. While the relative branching fractions depend both on the model type and on $\tan\beta$, the overall picture tends to be qualitatively similar (189). The most stringent constraints are obtained for $m_a < 3$ GeV, whereas the searches in the region $10 < m_a < 60$ GeV do not yet provide strong constraints on 2HDM+S predictions.

6.3. Higgs Triplet

For Higgs triplet models, the experimental focus has been on the Georgi–Machacek model (65). The specific signatures of this model are fermiophobic neutral, charged, and doubly charged Higgs bosons. The only practically relevant decay modes for these bosons are $H \to WW/ZZ$, $H^{\pm} \to WZ$, and $H^{\pm\pm} \to W^{\pm}W^{\pm}$ if kinematically allowed. Because of the fermiophobic nature of these additional Higgs bosons, the relevant production mode for all three states is VBF. ATLAS and CMS searches for these specific signatures are discussed above in Sections 3.1.1 and 3.3. Upper limits are set on the $\sin^2\Theta_H$ parameter, which sets the fraction of the gauge boson masses that are generated by the triplet Higgs fields, as a function of the mass of the considered heavy Higgs boson.

In addition to these searches, a global fit obtains various constraints on the parameter space using information from LHC results (190). Masses below 200 GeV were not investigated in any of the dedicated searches for the fermiophobic Higgs bosons and should be targeted by updates

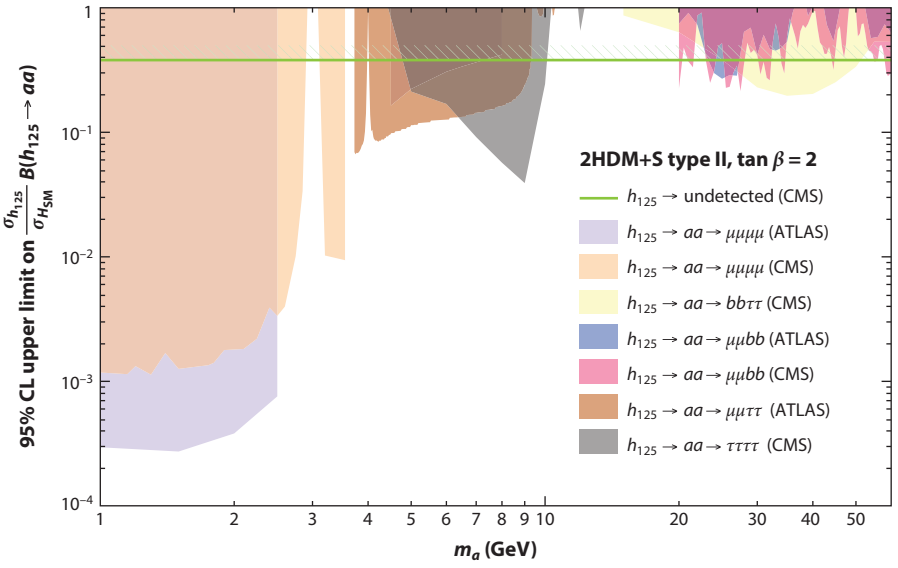

Figure 5

The 95% CL upper limit on $\frac{\sigma_{h_{125}}}{\sigma_{H_{SM}}} B(h_{125} \to aa)$ as a function of m_a in a type II 2HDM+S model with $\tan\beta = 2$ (branching fractions are from Reference 189). The considered final states are $\mu\mu\mu\mu$ (122, 123), $\tau\tau\tau\tau$ (125, 126), $\mu\mu bb$ (128, 129), $\mu\mu\tau\tau$ (124), and $bb\tau\tau$ (127). Also shown is the upper limit on the branching fraction of h_{125} to undetected particles from a combination of h_{125} measurements (154). Abbreviations: CL, confidence level; h_{125}, 125-GeV Higgs boson; 2HDM+S, two Higgs doublet model with a complex singlet.

of the searches. Another unexplored area is final states with photons, in particular the one-loop decay $H^{\pm} \to W\gamma$ (191).

7. OUTLOOK

The LHC revealed the existence of a Higgs boson that is consistent not only with a minimal Higgs sector as in the SM but also with extended scalar sectors, such as the Higgs sector of the MSSM and the NMSSM. Although the LHC data have so far not given any indications of the couplings being different from the predicted ones in the SM, there are good arguments for the Higgs sector being nonminimal. Precision measurements of the Higgs boson couplings at the HL-LHC, and in particular at a future e^+e^- collider, will lead to a sizable increase in the sensitivity to extended scalar sectors (192).

Numerous searches for additional neutral and charged Higgs bosons have been carried out at the LHC and have targeted a variety of models. With no significant excess observed, the experimental focus of the LHC and HL-LHC will be on three fronts. First, all searches are statistically limited and will profit significantly from more data. Second, the experimental collaborations strive to improve both the search strategies and the object reconstruction (e.g., with machine learning techniques), as demonstrated in several of the discussed searches. Third, uncovered processes and areas of phase space will be natural next targets (e.g., searches for nonstandard Higgs-to-Higgs decays). Beyond the lifetime of the LHC, direct searches for additional Higgs bosons at possible future lepton or hadron colliders will have a vastly increased yield in terms of both mass and couplings (192, 193).

DISCLOSURE STATEMENT

The author is not aware of any affiliations, memberships, funding, or financial holdings that might be perceived as affecting the objectivity of this review.

ACKNOWLEDGMENTS

Thanks to Cécile Caillol and Roger Wolf for providing numerical inputs on the CMS results and related discussions. Thanks to Huacheng Cai and Jeannette Lorenz for providing ATLAS numerical results and related information. Special thanks to Tania Robens and Tim Stefaniak for providing numerical results for the Higgs singlet summary and for related discussions. Thanks to Jan Kieseler, Artur Gottmann, and Roger Wolf for providing very useful feedback on a draft of this article.

LITERATURE CITED

1. Aad G, et al. (ATLAS Collab.) *Phys. Lett. B* 716:1 (2012)
2. Chatrchyan S, et al. (CMS Collab.) *Phys. Lett. B* 716:30 (2012)
3. Englert F, Brout R. *Phys. Rev. Lett.* 13:321 (1964)
4. Guralnik GS, Hagen CR, Kibble TWB. *Phys. Rev. Lett.* 13:585 (1964)
5. Higgs PW. *Phys. Rev.* 145:1156 (1966)
6. Aad G, et al. (ATLAS Collab.) *Phys. Rev. Lett.* 114:191803 (2015)
7. Aaboud M, et al. (ATLAS Collab.) *Phys. Lett. B* 784:345 (2018)
8. Sirunyan AM, et al. (CMS Collab.) *Phys. Lett. B* 805:135425 (2020)
9. Wilson KG. *Phys. Rev. D* 3:1818 (1971)
10. Giudice GF. *Proc. Sci.* EPS-HEP2013:163 (2013)
11. Ivanov IP. *Prog. Part. Nucl. Phys.* 95:160 (2017)
12. Englert C, et al. *J. Phys. G* 41:113001 (2014)
13. Dawson S, Englert C, Plehn T. *Phys. Rep.* 816:1 (2019)
14. Tanabashi M, et al. *Phys. Rev. D* 98:030001 (2018)
15. Djouadi A. *Phys. Rep.* 459:1 (2008)
16. Kim JE, Nilles HP. *Phys. Lett. B* 138:150 (1984)
17. Ellwanger U, Hugonie C, Teixeira AM. *Phys. Rep.* 496:1 (2010)
18. Maniatis M. *Int. J. Mod. Phys. A* 25:3505 (2010)
19. Lee TD. *Phys. Rev. D* 8:1226 (1973)
20. Branco GC, et al. *Phys. Rep.* 516:1 (2012)
21. Sikivie P, Susskind L, Voloshin MB, Zakharov VI. *Nucl. Phys. B* 173:189 (1980)
22. Peskin ME, Takeuchi T. *Phys. Rev. D* 46:381 (1992)
23. McDonald J. *Phys. Rev. D* 50:3637 (1994)
24. Schabinger RM, Wells JD. *Phys. Rev. D* 72:093007 (2005)
25. O'Connell D, Ramsey-Musolf MJ, Wise MB. *Phys. Rev. D* 75:037701 (2007)
26. Bahat-Treidel O, Grossman Y, Rozen Y. *J. High Energy Phys.* 0705:022 (2007)
27. Barger V, et al. *Phys. Rev. D* 79:015018 (2009)
28. Gunion JF, Haber HE. *Phys. Rev. D* 67:075019 (2003)
29. Bernon J, et al. *Phys. Rev. D* 92:075004 (2015)
30. Bernon J, et al. *Phys. Rev. D* 93:035027 (2016)
31. Gunion JF, Haber HE. *Nucl. Phys. B* 272:1 (1986). Erratum. *Nucl. Phys. B* 402:567 (1993)
32. Gunion JF, Haber HE. *Nucl. Phys. B* 278:449 (1986). Erratum. *Nucl. Phys. B* 402:569 (1993)
33. Haber HE, Hempfling R, Hoang AH. *Z. Phys. C* 75:539 (1997)
34. Heinemeyer S, Hollik W, Weiglein G. *Comput. Phys. Commun.* 124:76 (2000)
35. Degrassi G, et al. *Eur. Phys. J. C* 28:133 (2003)

36. Hahn T, et al. *Phys. Rev. Lett.* 112:141801 (2014)
37. Bahl H, et al. arXiv:1811.09073 [hep-ph] (2018)
38. Zwirner F. *Int. J. Mod. Phys. A* 1(Proc. Suppl. 1, A–B):309 (1993)
39. Sirunyan AM, et al. (CMS Collab.) *Eur. Phys. J. C* 80:3 (2020)
40. Aad G, et al. (ATLAS Collab.) *Phys. Rev. D* 101:032009 (2020)
41. ATLAS Collab. arXiv:1909.08457 [hep-ex] (2019)
42. Carena M, Low I, Shah NR, Wagner CEM. *J. High Energy Phys.* 1404:15 (2014)
43. Haber HE, Heinemeyer S, Stefaniak T. *Eur. Phys. J. C* 77:742 (2017)
44. Bagnaschi E, et al. *Eur. Phys. J. C* 79:617 (2019)
45. Bahl H, Liebler S, Stefaniak T. *Eur. Phys. J. C* 79:279 (2019)
46. Djouadi A, Quevillon J. *J. High Energy Phys.* 1310:28 (2013)
47. Djouadi A, et al. *Eur. Phys. J. C* 73:2650 (2013)
48. Maiani L, Polosa AD, Riquer V. *Phys. Lett. B* 724:274 (2013)
49. Djouadi A, et al. *J. High Energy Phys.* 1506:168 (2015)
50. Wells JD. arXiv:hep-ph/0306127 (2003)
51. Arkani-Hamed N, Dimopoulos S. *J. High Energy Phys.* 0506:073 (2005)
52. Giudice GF, Romanino A. *Nucl. Phys. B* 699:65 (2004). Erratum. *Nucl. Phys. B* 706:487 (2005)
53. Lee G, Wagner CEM. *Phys. Rev. D* 92:075032 (2015)
54. Bahl H, Hollik W. *J. High Energy Phys.* 1807:182 (2018)
55. He XG, et al. *Phys. Rev. D* 79:023521 (2009)
56. Grzadkowski B, Osland P. *Phys. Rev. D* 82:125026 (2010)
57. Logan HE. *Phys. Rev. D* 83:035022 (2011)
58. Chen CY, Freid M, Sher M. *Phys. Rev. D* 89:075009 (2014)
59. Muhlleitner M, Sampaio MOP, Santos R, Wittbrodt J. *J. High Energy Phys.* 1703:94 (2017)
60. Chalons G, Domingo F. *Phys. Rev. D* 86:115024 (2012)
61. Baum S, Shah NR. arXiv:1808.02667 [hep-ph] (2018); Baum S, Shah NR. *J. High Energy Phys.* 1812:44 (2018)
62. Barbieri R, et al. *Phys. Rev. D* 87:115018 (2013)
63. Baum S, Freese K, Shah NR, Shakya B. *Phys. Rev. D* 95:115036 (2017)
64. Baglio J, et al. *J. High Energy Phys.* 1304:151 (2013)
65. Georgi H, Machacek M. *Nucl. Phys. B* 262:463 (1985)
66. Chanowitz MS, Golden M. *Phys. Lett. B* 165:105 (1985)
67. Chiang CW, Tsumura K. *J. High Energy Phys.* 1504:113 (2015)
68. Chiang CW, Kuo AL, Yagyu K. *Phys. Lett. B* 774:119 (2017)
69. Aaboud M, et al. (ATLAS Collab.) *Eur. Phys. J. C* 78:903 (2018)
70. Sirunyan AM, et al. (CMS Collab.) *J. Instrum.* 14:P07004 (2019)
71. ATLAS Collab. *Luminosity determination in* pp *collisions at* $\sqrt{s} = 13$ *TeV using the ATLAS detector at the LHC*. ATLAS Conf. Note ATLAS-CONF-2019-021, CERN, Geneva (2019)
72. CMS Collab. *CMS luminosity measurement for the 2018 data-taking period at* $\sqrt{s} = 13$ *TeV*. CMS Phys. Anal. Summ. CMS-PAS-LUM-18-002, CERN, Geneva (2019)
73. Aaboud M, et al. (ATLAS Collab.) *Eur. Phys. J. C* 78:24 (2018)
74. Sirunyan AM, et al. (CMS Collab.) *J. High Energy Phys.* 2003:34 (2020)
75. Aaboud M, et al. (ATLAS Collab.) *Eur. Phys. J. C* 78:293 (2018)
76. Aaboud M, et al. (ATLAS Collab.) *J. High Energy Phys.* 1803:9 (2018)
77. Sirunyan AM, et al. (CMS Collab.) *J. High Energy Phys.* 1806:127 (2018). Erratum. *J. High Energy Phys.* 1903:128 (2019)
78. Khachatryan V, et al. (CMS Collab.) *Eur. Phys. J. C* 74:3076 (2014)
79. Aaboud M, et al. (ATLAS Collab.) *Phys. Lett. B* 775:105 (2017)
80. Sirunyan AM, et al. (CMS Collab.) *Phys. Rev. D* 98:092001 (2018)
81. Sirunyan AM, et al. (CMS Collab.) *Phys. Lett. B* 793:320 (2019)
82. ATLAS Collab. *Search for resonances in the 65 to 110 GeV diphoton invariant mass range using 80* fb^{-1} *of* pp *collisions collected at* $\sqrt{s} = 13$ *TeV with the ATLAS detector*. ATLAS Conf. Note ATLAS-CONF-2018-025, CERN, Geneva (2018)

83. Cao J, et al. *Phys. Rev. D* 95:116001 (2017)
84. Fox PJ, Weiner N. *J. High Energy Phys.* 1808:25 (2018)
85. Biekötter T, Chakraborti M, Heinemeyer S. *Eur. Phys. J. C* 80:2 (2020)
86. Aaboud M, et al. (ATLAS Collab.) *J. High Energy Phys.* 1801:55 (2018)
87. Sirunyan AM, et al. (CMS Collab.) *J. High Energy Phys.* 1809:7 (2018)
88. Aad G, et al. arXiv:2002.12223 [hep-ex] (2020)
89. Aad G, et al. (ATLAS Collab.) *Eur. Phys. J. C* 76:295 (2016)
90. Sirunyan AM, et al. (CMS Collab.) *J. Instrum.* 13:P10005 (2018)
91. Sirunyan AM, et al. (CMS Collab.) *J. High Energy Phys.* 2003:55 (2020)
92. Gaemers KJF, Hoogeveen F. *Phys. Lett. B* 146:347 (1984)
93. Dicus D, Stange A, Willenbrock S. *Phys. Lett. B* 333:126 (1994)
94. Bernreuther W, Flesch M, Haberl P. *Phys. Rev. D* 58:114031 (1998)
95. Bernreuther W, et al. *Phys. Rev. D* 93:034032 (2016)
96. Carena M, Liu Z. *J. High Energy Phys.* 1611:159 (2016)
97. Aaboud M, et al. (ATLAS Collab.) *Phys. Rev. Lett.* 119:191803 (2017)
98. Sirunyan AM, et al. (CMS Collab.) *J. High Energy Phys.* 2004:171 (2020)
99. Sirunyan AM, et al. (CMS Collab.) *Eur. Phys. J. C* 80:75 (2020)
100. Sirunyan AM, et al. (CMS Collab.) *J. High Energy Phys.* 1808:113 (2018)
101. ATLAS Collab. arXiv:1907.02749 [hep-ex] (2019)
102. Aaboud M, et al. (ATLAS Collab.) *J. High Energy Phys.* 1907:117 (2019)
103. Sirunyan AM, et al. (CMS Collab.) *Phys. Lett. B* 798:134992 (2019)
104. Sirunyan AM, et al. (CMS Collab.) *J. High Energy Phys.* 1905:210 (2019)
105. Sirunyan AM, et al. (CMS Collab.) *J. High Energy Phys.* 1711:10 (2017)
106. Lees JP, et al. *Phys. Rev. D* 87:031102 (2013). Erratum. *Phys. Rev. D* 87:059903 (2013)
107. Sirunyan AM, et al. (CMS Collab.) *Phys. Lett. B* 788:7 (2019)
108. Aaboud M, et al. (ATLAS Collab.) *J. High Energy Phys.* 1811:40 (2018)
109. Sirunyan AM, et al. (CMS Collab.) *Phys. Lett. B* 778:101 (2018)
110. Aaboud M, et al. (ATLAS Collab.) *Phys. Rev. Lett.* 121:191801 (2018). Erratum. *Phys. Rev. Lett.* 122:089901 (2019)
111. Aaboud M, et al. (ATLAS Collab.) *J. High Energy Phys.* 1901:30 (2019)
112. Sirunyan AM, et al. (CMS Collab.) *J. High Energy Phys.* 1808:152 (2018)
113. Sirunyan AM, et al. (CMS Collab.) *J. High Energy Phys.* 1801:54 (2018)
114. Aaboud M, et al. (ATLAS Collab.) *J. High Energy Phys.* 1904:92 (2019)
115. Aaboud M, et al. (ATLAS Collab.) *J. High Energy Phys.* 1905:124 (2019)
116. Aaboud M, et al. (ATLAS Collab.) *Eur. Phys. J. C* 78:1007 (2018)
117. Aad G. (ATLAS Collab.) *Phys. Lett. B* 800:135103 (2020)
118. Aaboud M, et al. (ATLAS Collab.) *J. High Energy Phys.* 1803:174 (2018). Erratum. *J. High Energy Phys.* 1811:51 (2018)
119. Sirunyan AM, et al. (CMS Collab.) *Eur. Phys. J. C* 79:564 (2019)
120. Sirunyan AM, et al. (CMS Collab.) *J. High Energy Phys.* 2003:65 (2020)
121. Aaboud M, et al. (ATLAS Collab.) *Phys. Lett. B* 783:392 (2018)
122. Aaboud M, et al. (ATLAS Collab.) *J. High Energy Phys.* 1806:166 (2018)
123. Sirunyan AM, et al. (CMS Collab.) *Phys. Lett. B* 796:131 (2019)
124. Aad G, et al. (ATLAS Collab.) *Phys. Rev. D* 92:052002 (2015)
125. Sirunyan AM, et al. (CMS Collab.) *Phys. Lett. B* 800:135087 (2020)
126. Sirunyan AM, et al. (CMS Collab.) *J. High Energy Phys.* 1811:18 (2018)
127. Sirunyan AM, et al. (CMS Collab.) *Phys. Lett. B* 785:462 (2018)
128. Aaboud M, et al. (ATLAS Collab.) *Phys. Lett. B* 790:1 (2019)
129. Sirunyan AM, et al. (CMS Collab.) *Phys. Lett. B* 795:398 (2019)
130. Aaboud M, et al. (ATLAS Collab.) *J. High Energy Phys.* 1810:31 (2018)
131. Aaboud M, et al. (ATLAS Collab.) *Phys. Lett. B* 782:750 (2018)
132. Aad G, et al. (ATLAS Collab.) *Eur. Phys. J. C* 76:210 (2016)

133. Curtin D, et al. *Phys. Rev. D* 90:075004 (2014)
134. Degrande C, et al. *Phys. Lett. B* 772:87 (2017)
135. CMS Collab. *Search for a light charged Higgs boson in the $H^{\pm} \to cs$ channel at 13 TeV*. CMS Phys. Anal. Summ. CMS-PAS-HIG-18-021, CERN, Geneva (2019)
136. Sirunyan AM, et al. (CMS Collab.) *J. High Energy Phys.* 1811:115 (2018)
137. Sirunyan AM, et al. (CMS Collab.) *Phys. Rev. Lett.* 123:131802 (2019)
138. Aaboud M, et al. (ATLAS Collab.) *J. High Energy Phys.* 1809:139 (2018)
139. Sirunyan AM, et al. (CMS Collab.) *J. High Energy Phys.* 1907:142 (2019)
140. Aaboud M, et al. (ATLAS Collab.) *J. High Energy Phys.* 1811:85 (2018)
141. Sirunyan AM, et al. (CMS Collab.) *J. High Energy Phys.* 2001:96 (2020)
142. CMS Collab. arXiv:2001.07763 [hep-ex] (2020)
143. Sirunyan AM, et al. (CMS Collab.) *Phys. Rev. Lett.* 119:141802 (2017)
144. Aaboud M, et al. (ATLAS Collab.) *Phys. Lett. B* 787:68 (2018)
145. Sirunyan AM, et al. (CMS Collab.) *Phys. Rev. Lett.* 120:081801 (2018)
146. Aaboud M, et al. (ATLAS Collab.) *Eur. Phys. J. C* 79:58 (2019)
147. Aaboud M, et al. (ATLAS Collab.) *Eur. Phys. J. C* 78:199 (2018)
148. Chao W, Si ZG, Xing ZZ, Zhou S. *Phys. Lett. B* 666:451 (2008)
149. Bambhaniya G, et al. *J. High Energy Phys.* 1405:33 (2014)
150. Hurth T. *Rev. Mod. Phys.* 75:1159 (2003)
151. Paul A, Straub DM. *J. High Energy Phys.* 1704:27 (2017)
152. Misiak M, Steinhauser M. *Eur. Phys. J. C* 77:201 (2017)
153. Bechtle P, et al. *Eur. Phys. J. C* 77:67 (2017)
154. Sirunyan AM, et al. (CMS Collab.) *Eur. Phys. J. C* 79:421 (2019)
155. Aad G, et al. (ATLAS Collab.) *Phys. Rev. D* 101:012002 (2020)
156. Bechtle P, et al. *Eur. Phys. J. C* 74:2711 (2014)
157. Stål O, Stefaniak T. *Proc. Sci.* EPS-HEP2013:314 (2013)
158. Bechtle P, et al. *J. High Energy Phys.* 1411:39 (2014)
159. de Florian D, et al., eds. *Handbook of LHC Higgs Cross Sections: 4. Deciphering the Nature of the Higgs Sector*, Vol. 2. Geneva: CERN. **https://e-publishing.cern.ch/index.php/CYRM/issue/view/32** (2017)
160. Berger EL, Han T, Jiang J, Plehn T. *Phys. Rev. D* 71:115012 (2005)
161. Dittmaier S, Kramer M, Spira M, Walser M. *Phys. Rev. D* 83:055005 (2011)
162. Flechl M, et al. *Phys. Rev. D* 91:075015 (2015)
163. Degrande C, Ubiali M, Wiesemann M, Zaro M. *J. High Energy Phys.* 1510:145 (2015)
164. Athron P, et al. *Eur. Phys. J. C* 77:879 (2017)
165. Bagnaschi E, et al. *Eur. Phys. J. C* 78:256 (2018)
166. Staub F. *Phys. Lett. B* 776:407 (2018)
167. Funk G, O'Neil D, Winters RM. *Int. J. Mod. Phys. A* 27:1250021 (2012)
168. Haller J, et al. *Eur. Phys. J. C* 78:675 (2018)
169. Enomoto T, Watanabe R. *J. High Energy Phys.* 1605:2 (2016)
170. Amhis YS, et al. arXiv:1909.12524 [hep-ex] (2019)
171. Haber HE, Stål O. *Eur. Phys. J. C* 75:491 (2015). Erratum. *Eur. Phys. J. C* 76:312 (2016)
172. Kling F, No JM, Su S. *J. High Energy Phys.* 1609:93 (2016)
173. Arbey A, Mahmoudi F, Stål O, Stefaniak T. *Eur. Phys. J. C* 78:182 (2018)
174. Chowdhury D, Eberhardt O. *J. High Energy Phys.* 1805:161 (2018)
175. Belyaev A, et al. *Phys. Rev. D* 97:035011 (2018)
176. López-Val D, Robens T. *Phys. Rev. D* 90:114018 (2014)
177. Robens T, Stefaniak T. *Eur. Phys. J. C* 75:104 (2015)
178. Robens T, Stefaniak T. *Eur. Phys. J. C* 76:268 (2016)
179. Ilnicka A, Robens T, Stefaniak T. *Mod. Phys. Lett. A* 33:1830007 (2018)
180. Robens T. *Proc. Sci.* LHCP2019:138 (2019)
181. Bechtle P, et al. *Comput. Phys. Commun.* 181:138 (2010)
182. Bechtle P, et al. *Comput. Phys. Commun.* 182:2605 (2011)

183. Bechtle P, et al. *Proc. Sci.* CHARGED2012:024 (2012)
184. Bechtle P, et al. *Eur. Phys. J. C* 74:2693 (2014)
185. Lewis IM, Sullivan M. *Phys. Rev. D* 96:035037 (2017)
186. King SF, Muhlleitner M, Nevzorov R. *Nucl. Phys. B* 860:207 (2012)
187. Ellwanger U, Rodríguez-Vázquez M. *J. High Energy Phys.* 1711:8 (2017)
188. Ellwanger U, Rodríguez-Vázquez M. *J. High Energy Phys.* 1602:96 (2016)
189. Haisch U, Kamenik JF, Malinauskas A, Spira M. *J. High Energy Phys.* 1803:178 (2018)
190. Chiang CW, Cottin G, Eberhardt O. *Phys. Rev. D* 99:015001 (2019)
191. Logan HE, Wu Y. *J. High Energy Phys.* 1811:121 (2018)
192. Ellis RK, et al. (Eur. Strategy Part. Phys. Prep. Group) arXiv:1910.11775 [hep-ex] (2019)
193. Cepeda M, et al. arXiv:1902.00134 [hep-ph] (2019)

Annual Review of Nuclear and Particle Science

Volume 70, 2020

Contents

Errata

An online log of corrections to *Annual Review of Nuclear and Particle Science* articles may be found at http://www.annualreviews.org/errata/nucl